A Rotating Speed Controller Design Method for Power Levelling by Means of Inertia Energy in Wind Power Systems

Qin, Zian; Blaabjerg, Frede; Loh, Poh Chiang

Published in:
I E E E Transactions on Energy Conversion

DOI (link to publication from Publisher):
10.1109/TEC.2015.2416004

Publication date:
2015

Document Version
Early version, also known as pre-print

A Rotating Speed Controller Design Method for Power Levelling by Means of Inertia energy in Wind Power Systems

Qin, Zian; Blaabjerg, Frede; Loh, Poh Chiang

Published in:
IEEE Transactions on Energy Conversion

DOI (link to publication from Publisher):

Publication date:
2014

A Rotating Speed Controller Design Method for Power Levelling by Means of Inertia Energy in Wind Power Systems

Zian Qin, *Student Member, IEEE,* Frede Blaabjerg, *Fellow, IEEE,* Poh Chiang Loh

***Abstract*—Power fluctuation caused by wind speed variations may be harmful for the stability of the power system as well as the reliability of the wind power converter, since it may induce thermal excursions in the solder joints of the power modules. Using the wind turbine rotor inertia energy for power levelling has been studied before, but no quantified analysis or generic design method have been found. In this paper, the transfer functions from the wind speed to electrical power, electromagnetic torque and rotating speed are built, based on which the rotating speed controller is designed in the frequency domain for power levelling. Moreover, the impact of other parameters on power levelling, including the time constant of MPPT and the rotor inertia, are also studied. With the proposed optimal design, the power fluctuations are mitigated as much as possible, while the stability of the rotating speed is still guaranteed. Moreover, the oscillation of the electromagnetic torque is also reduced, and the performance of the MPPT is only weakened slightly.**

***Keywords*—wind power converter; power levelling; transfer function; inertia energy.**

I. Introduction

WIND power has developed very fast during the last decades [1]–[3] and it has achieved a large penetration of the electricity consumption in some countries, for example, 53% experienced in Spain [4] and more than 40% in Denmark. Moreover, with the setting of EUs 20-20-20 goals and Danish agreement that 50% of the electricity consumption will be supplied by wind power in 2020 [5], the wind turbine technology will go even further. As a result, the fluctuation of wind power becomes a more important issue, because it will not only influence the stability of the power system but also reduce the reliability of the wind power converter.

In order to achieve a low wind energy price per kWh by reducing the maintenance cost of the wind turbine system, the reliability of the large-scale wind turbine has drawn much attention [6]–[8]. The lifetime of the power modules used in the wind power converter is found to be inversely proportional to the temperature swing ΔT in the solder joints [9], [10]. The ΔT is mainly caused by the power fluctuations, which is due to the inherent characteristic of the wind nature. Therefore, the power levelling is a kind of solution to reduce the ΔT.

To smooth the power fluctuations by adding Energy Storage Systems (ESSs) like flywheels, supercapacitors, and batteries [11]–[14] in wind power converters has been proposed. The ESS is normally connected to the DC link and operate as a buffer by absorbing or releasing power when the wind power is above or below average value. The ESS will therefore not influence the wind turbine control, and the main efforts in this method are put into the topologies, control strategies, and size evaluation of the ESS [15]–[17]. The high power generation efficiency is retained and the power fluctuation can be mitigated significantly as long as a large enough ESS is introduced. A commercially available wind turbine with ESS integrated already exists [18], Despite, the drawbacks are obvious, e.g. the power fluctuations and thermal excursions in the generator side converter cannot be improved by the ESS connected on the DC link, and the cost of ESS for the large-scale wind turbines is still very high [19]. It is thus essential to first study how much the the wind turbine system itself can contribute to relieve the power fluctuations.

Pitch angle control and DC-link voltage control have been studied for the power levelling [20]–[22]. However, changing the pitch angle below the nominal wind speed will loss the power generation considerably. Regulating the DC-link voltage could be an effective approach for low-voltage-ride-through, but it is negligible for the power levelling in the normal condition. Another possibility for power levelling in large-scale wind power systems is the rotor, which has a larger inertia of moment storing big amount of energy that can be used as an ESS for power levelling [23]–[29]. This inertia energy is indirectly controlled by regulating the rotating speed of the wind turbine. The related control strategies have been studied in [23], [24], however detailed analysis was not given and the stability of the rotating speed was not considered. Advanced control methods like Fuzzy Control and Model Predictive Control have been employed for power levelling [25], [26]. The approaches perform well and the constraint of the rotating speed is also studied. Despite, the control methods were relatively complicated and the generic design approach was still missing. In [30], the constant power control, constant torque control, and optimal power control were comparably studied from power levelling point of view, then a transfer function from wind speed to the electrical power was derived to illustrate the power filtering effect and analyze the stability of the controllers as well. The transfer function in frequency domain made the filtering effect much easier to be understood and the conclusion that the power levelling was a matter to design the slop between the electrical power and rotating speed was very valuable. Nevertheless, an optimal design

Z. Qin, F. Blaabjerg and P. C. Loh are with the Department of Energy Technology, Aalborg University, Aalborg 9220, Denmark. E-mail: zqi@et.aau.dk, fbl@et.aau.dk, pcl@et.aau.dk

of the rotating speed control in frequency domain was not given. Some details were also ignored in the derivation of the transfer function, in terms of the MPPT controller, and the impact of the rotor inertia. Moreover, the influence to the torque was not considered, which may be significantly changed by the power levelling strategies.

In this paper, the transfer functions from the wind speed to electrical power, torque, and rotating speed are built first. Then the rotating speed controller is optimally designed in frequency domain and the stability of the rotating speed is studied and guaranteed. Moreover, the impact on the torque as well as the sensitivity to the other parameters like the inertia, the time constant of the MPPT controller are also analyzed. The paper is organized as follows: Section II illustrates the system model. The rotating speed controller is designed in Section III. The impact of the other parameters on the power levelling is studied in Section IV. In Section V, the proposed method is verified by the simulation results. The conclusion comes in Section VI.

II. System Modelling

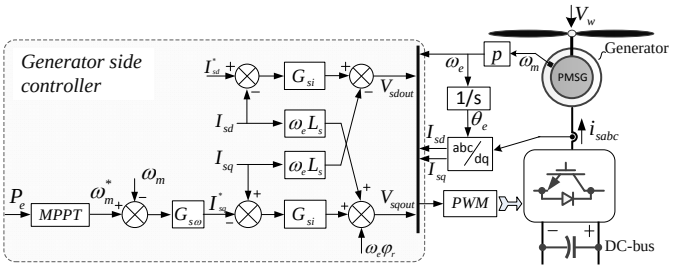

Fig. 1. A PMSG based direct-drive wind power generator and its drive drain.

The system is modelled first, in terms of the wind turbine model and the generator model, as shown in Fig. 1. The generator side converter model is usually equivalent to a delay. The delay time is only 0.75 of the switching period [31], which is much shorter than the time constant of the wind turbine model and generator model, thus it is ignored. The grid side converter is not considered since the grid side converter is just tracking the power of the generator side converter. It should be noted that all the parameter values are listed in Appendix A.

A. Wind turbine model

The wind power absorbed by the turbine can be expressed as,

$$P_W = C_p \frac{\rho A}{2} V_W^3 \tag{1}$$

where ρ denotes the air density, $A = \pi R^2$ is the turbine swept area, R is the radius of the blade, V_W indicates the wind speed, C_p is the power coefficient of the blades, which is defined as,

$$\begin{cases} C_p(\lambda,\beta) = c_1(c_2/\lambda_i - c_3\beta - c_4)e^{-c_5/\lambda_i} + c_6\lambda \\ \frac{1}{\lambda_i} = \frac{1}{\lambda+0.08\beta} - \frac{0.035}{\beta^3+1} \\ \lambda = \frac{\omega_m R}{V_W} \end{cases} \tag{2}$$

where λ is the tip speed ratio, and β is the pitch angle, $c_1 \sim c_6$ are the coefficients, and ω_m is the rotating speed. The maximum power coefficient $C_{p,opt}$ is 0.48, which can be obtained when the optimal tip speed ratio $\lambda_{opt} = 8.1$ and zero pitch angle $\beta = 0$ are achieved. The wind power can also be expressed as,

$$P_W = T_m \omega_m \tag{3}$$

where T_m is the aerodynamic torque on the turbine and it can be expressed as the following by substituting (1) into (3),

$$T_m = C_p \frac{\rho A V_W^3}{2\omega_m} \tag{4}$$

Equation (4) is actually the aerodynamic model of the wind turbine, which can be used to obtain the aerodynamic torque based on the wind speed, the rotating speed and the characteristics of the wind turbine.

B. Generator model

For the PMSG based wind power generator, the electrical, torque and mechanical equations are expressed in the following. In the rotating frame (dq), the q-axis is aligned with the rotor flux.

$$v_{sd} = R_s I_{sd} + L_s \frac{dI_{sd}}{dt} - \omega_e L_s I_{sq} \tag{5}$$

$$v_{sq} = R_s I_{sq} + L_s \frac{dI_{sq}}{dt} + \omega_e L_s I_{sd} + \omega_e \varphi_r \tag{6}$$

$$T_e = \frac{3p}{2} \varphi_r I_{sq} \tag{7}$$

$$J \frac{d\omega_m}{dt} = T_m - T_e \tag{8}$$

where v_{sd} and v_{sq} are the stator voltages, i_{sd} and i_{sq} are the stator currents in dq frame, L_s and R_s are the stator inductance and resistance, respectively, φ_r is the rotor flux, T_e is the electromagnetic torque, p is the machine pole pairs, $\omega_e = p\omega_m$ is the electrical rotating speed, and J is the rotor inertia including the turbine and the generator. The friction is not the dominant factor and it is ignored here. The generator side controller is a conventional dq frame control, and the compensation terms are based on the generator model, as seen in Fig. 1. The outer and inner loop are the rotating speed control and stator current control, respectively. The reference of d-axis is zero.

III. Design of the Rotating Speed Controller

As known, the kinetic energy stored in the rotor can be expressed as,

$$E_m = \frac{1}{2} J \omega_m^2 \tag{9}$$

and the charging/discharging power of the turbine can be obtained as the following,

$$P_m = \frac{dE_m}{dt} = \frac{d}{dt}\left(\frac{1}{2} J \omega_m^2\right) = J\omega_m \frac{d\omega_m}{dt} \tag{10}$$

As seen in (10), the charging/discharging power of the turbine does not only relate to the rotating speed ω_m but also to the speed change rate $d\omega_m/dt$. Thus, $d\omega_m/dt$ can be regulated for

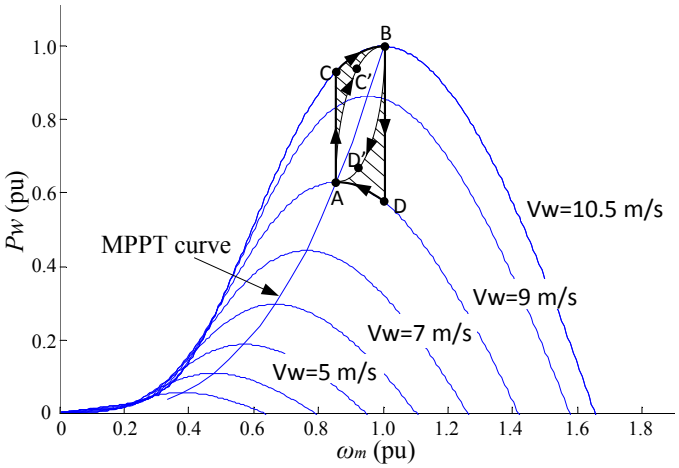

Fig. 2. The behaviour of the wind turbine in a wind speed step.

the power levelling according to the basic relationship between the wind power P_W, the charging/discharging power of the turbine P_m and the electrical power delivered by the drive train P_e, as following,

$$P_e = P_W - P_m \tag{11}$$

which is also indicated in Fig.2. In steady state, the wind turbine operates on the MPPT curve to maximize the power generation. Assuming there is a wind speed step between 9 m/s and 10.5 m/s, the wind power P_W obtained by the turbine will follow the curve $\boldsymbol{ACB}$ in increasing and $\boldsymbol{BDA}$ in decreasing. The power changes fast and even an overshoot happens in step-down of the wind speed, which is not desired to happen in electrical power P_e. In order to obtain a smoother electrical power, for example following the curves $\boldsymbol{AC'B}$ and $\boldsymbol{BD'A}$, the charging/discharging power P_m of the turbine is needed to compensate the difference indicated by the shadow. The P_m is indirectly regulated by the rotating speed controller, which is therefore designed by the following.

The transfer function from the wind speed to the electrical power is built first for the design. Since the relationship between the wind speed and the electrical power is non-linear in the whole wind speed range, the small perturbation linearization is relatively more appropriate for the transfer function. The corresponding dimensionless transfer functions have been partial derived in [30] and they are expressed as the following,

$$G_{P/V}(s) = \frac{\Delta\tilde{P}_e(s)}{\Delta\tilde{V}_W(s)} = \frac{(3-\lambda_0 C'_{p0}/C_{p0})(\omega_{m0}/P_{W0})slope}{\tau_0 s - \lambda_0 C'_{p0}/C_{p0} + (\omega_{m0}/P_{W0})slope} \tag{12}$$

$$G_{\omega/V}(s) = \frac{\Delta\tilde{\omega}_m(s)}{\Delta\tilde{V}_W(s)} = \frac{(3-\lambda_0 C'_{p0}/C_{p0})}{\tau_0 s - \lambda_0 C'_{p0}/C_{p0} + (\omega_{m0}/P_{W0})slope} \tag{13}$$

where $\Delta\tilde{P}_e = \Delta P_e/P_{e0}$, $\Delta\tilde{V}_W = \Delta V_W/V_{W0}$, $\Delta\tilde{\omega}_m = \Delta\omega_m/\omega_{m0}$, $\lambda_0 = \omega_{m0}R/V_{W0}$, $C_{p0} = C_p(\lambda_0)$, $C'_{p0} = dC_p(\lambda)/d\lambda|_{\lambda_0}$, $\tau_0 = J\omega_{m0}^2/P_{W0}$, X_0 ($X = P_e$, V_W, $\omega_m \cdots$) indicate the static values of the parameters and the $slope$ is

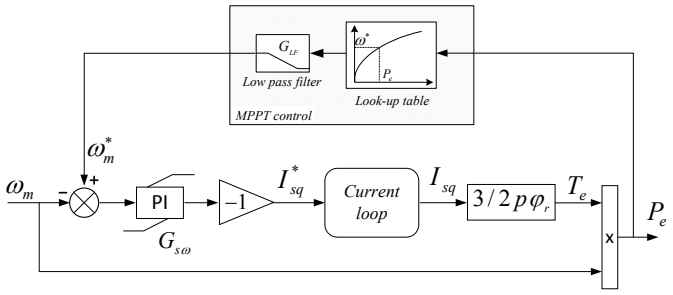

Fig. 3. The relationship between the rotating speed and electrical power with MPPT control.

defined as,

$$slope = \frac{\partial P_e}{\partial \omega_m} \tag{14}$$

According to generator side controller (see Fig. 1), the torque equation (7) and the static equation $P_e = T_e\omega_m$, the relationship between ω_m and P_e can be indicated as shown in Fig.3, where ω_m^* is the reference of the rotating speed and the low pass filter in MPPT control is expressed as,

$$G_{LF} = \frac{1}{sT_{mppt}+1} \tag{15}$$

According to Fig. 3, it is obtained,

$$P_{e0} + \Delta P_e = (T_{e0} + \Delta T_e)(\omega_{m0} + \Delta\omega_m) \tag{16}$$

Removing the static and the second-order small terms, it can be gained,

$$\Delta P_e = T_{e0}\Delta\omega_m + \Delta T_e\omega_{m0} \tag{17}$$

where ΔT_e can be obtained according to Fig. 3,

$$\Delta T_e = (\Delta\omega_m - \Delta\omega_m^*)G_{s\omega}\frac{3}{2}p\varphi_r \tag{18}$$

According to (1) and (2), the MPPT control can be expressed as,

$$\omega_m^* = \frac{\lambda_{opt}}{R}\left(\frac{2P_e}{\rho A C_{p,opt}}\right)^{1/3} G_{LF} \tag{19}$$

Then it can be derived,

$$\Delta\omega_m^* = \frac{\partial\omega_m^*}{\partial P_e}\Delta P_e = \frac{\lambda_{opt}}{3R}G_{LF}\left(\frac{2}{\rho A C_{p,opt}}\right)^{1/3} P_{e0}^{-2/3}\Delta P_e \tag{20}$$

Substituting static expression of (19) into (20), it can be obtained,

$$\Delta\omega_m^* = \frac{\omega_{m0}}{3P_{e0}}G_{LF}\Delta P_e \tag{21}$$

Substituting (18) and (21) into (17), it is obtained,

$$slope = \frac{\Delta P_e}{\Delta\omega_m} = \frac{T_{e0} + \frac{3}{2}p\varphi_r\omega_{m0}G_{s\omega}}{1 + \frac{3}{2}p\varphi_r\omega_{m0}G_{s\omega}\cdot\frac{\omega_{m0}}{3P_{e0}}G_{LF}} \tag{22}$$

The rotating speed controller is a typical Proportional+Integration (PI) controller, which can be expressed as,

$$G_{s\omega} = K_{p\omega} + \frac{K_{i\omega}}{s} \tag{23}$$

Substituting (1), (22) and (23) into (12), and considering that $C'_{p0} = 0$ when C_{p0} achieves its maximum value, it is gained,

$$G_{P/V}(s) = \frac{\frac{3}{J}(k_2\omega_{m0}+k_1K_{p\omega})s+\frac{3k_1K_{i\omega}}{J}}{s^2+\left(\frac{k_1}{3k_2\omega_{m0}}\frac{sK_{p\omega}+K_{i\omega}}{sT_{mppt}+1}+\frac{k_2\omega_{m0}}{J}+\frac{k_1K_{p\omega}}{J}\right)s+\frac{k_1K_{i\omega}}{J}} \tag{24}$$

where $k_1 = \frac{3}{2}p\varphi_r$, $k_2 = \frac{\rho AC_{p,opt}R^3}{2\lambda^3_{opt}}$. As seen the dimensionless transfer function from wind speed to electrical power is actually a third-order and it can be simplified to a second-order, if the condition can be achieved,

$$K_{p\omega} = T_{mppt} * K_{i\omega} \tag{25}$$

Thus, (24) can be simplified to,

$$G_{P/V}(s) = \frac{\frac{3}{J}(k_2\omega_{m0} + k_1K_{i\omega}T_{mppt})s + \frac{3k_1K_{i\omega}}{J}}{s^2 + \left(\frac{k_1K_{i\omega}}{3k_2\omega_{m0}} + \frac{k_2\omega_{m0}}{J} + \frac{k_1K_{i\omega}T_{mppt}}{J}\right)s + \frac{k_1K_{i\omega}}{J}} \tag{26}$$

The transfer function becomes a second-order model with a lead compensation and it can also be expressed as,

$$G_{P/V}(s) = K_1\frac{s+\omega_{f1}}{s^2+2\zeta\omega_0 s+\omega_0^2} \tag{27}$$

where K_1, ω_{f1}, ξ and ω_0 can be indicated as,

$$\begin{cases} K_1 = \frac{3}{J}(k_2\omega_{m0} + k_1K_{i\omega}T_{mppt}) \\ \omega_{f1} = \frac{k_1K_{i\omega}}{k_2\omega_{m0}+k_1K_{i\omega}T_{mppt}} \\ \omega_0 = \sqrt{k_1K_{i\omega}/J} \\ \zeta = \frac{\frac{k_1K_{i\omega}}{3k_2\omega_{m0}}+\frac{k_2\omega_{m0}}{J}+\frac{k_1K_{i\omega}T_{mppt}}{J}}{2\sqrt{k_1K_{i\omega}/J}} \end{cases} \tag{28}$$

Another two important indicators are the mechanical stress and variation of the rotating speed, which can be analyzed by $G_{T/V}(s)$ and $G_{\omega/V}(s)$, respectively. Substituting (1), (22), (23) and (25) into (13), and considering that $C'_{p0} = 0$ when C_{p0} achieves its maximum value, it is obtained as,

$$G_{\omega/V}(s) = \frac{\frac{3k_2\omega_{m0}}{J}s + \frac{k_1K_{i\omega}}{J}}{s^2 + \left(\frac{k_1K_{i\omega}}{3k_2\omega_{m0}} + \frac{k_2\omega_{m0}}{J} + \frac{k_1K_{i\omega}T_{mppt}}{J}\right)s + \frac{k_1K_{i\omega}}{J}} \tag{29}$$

which can also be shortened to,

$$G_{\omega/V}(s) = K_2\frac{s+\omega_{f2}}{s^2+2\zeta\omega_0 s+\omega_0^2} \tag{30}$$

where K_2 and ω_{f2} are,

$$\begin{cases} K_2 = \frac{3k_2\omega_{m0}}{J} \\ \omega_{f2} = \frac{k_1K_{i\omega}}{3k_2\omega_{m0}} \end{cases} \tag{31}$$

The dimensionless transfer function from wind speed to the electromagnetic torque is defined as,

$$G_{T/V}(s) = \frac{\Delta\tilde{T}_e(s)}{\Delta\tilde{V}_W(s)} = \frac{\Delta T_e}{\Delta V_W}\cdot\frac{V_{W0}}{T_{e0}} \tag{32}$$

Substituting (17) into (32), it can be obtained,

$$G_{T/V}(s) = \frac{\Delta P_e - T_{e0}\Delta\omega_m}{\omega_{m0}T_{e0}}\cdot\frac{V_{W0}}{\Delta V_W} = \frac{\Delta\tilde{P}_e(s)}{\Delta\tilde{V}_W(s)} - \frac{\Delta\tilde{\omega}_m(s)}{\Delta\tilde{V}_W(s)} \tag{33}$$

Substituting (26) and (29) into (33), it is acquired,

$$G_{T/V}(s) = \frac{\frac{3k_1K_{i\omega}T_{mppt}}{J}s + \frac{2k_1K_{i\omega}}{J}}{s^2 + \left(\frac{k_1K_{i\omega}}{3k_2\omega_{m0}} + \frac{k_2\omega_{m0}}{J} + \frac{k_1K_{i\omega}T_{mppt}}{J}\right)s + \frac{k_1K_{i\omega}}{J}} \tag{34}$$

Similarly, $G_{T/V}(s)$ can be expressed as,

$$G_{T/V}(s) = K_3\frac{s+\omega_{f3}}{s^2+2\zeta\omega_0 s+\omega_0^2} \tag{35}$$

where K_3 and ω_{f3} can be indicated as,

$$\begin{cases} K_3 = \frac{3k_1K_{i\omega}T_{mppt}}{J} \\ \omega_{f3} = \frac{2}{3T_{mppt}} \end{cases} \tag{36}$$

According to (27), (30) and (35), $G_{P/V}(s)$, $G_{T/V}(s)$ and

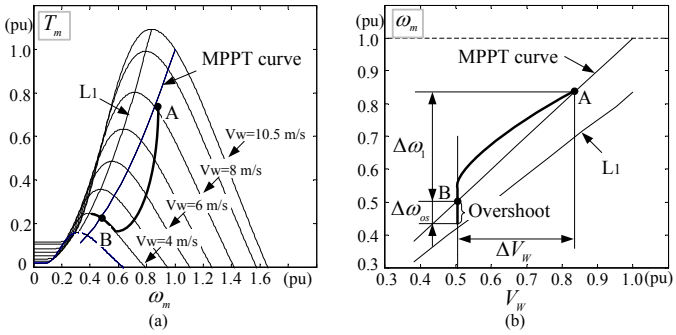

Fig. 4. Illustration for the stable region of the wind turbine (a) mechanical torque vs. rotating speed (b) rotating speed vs. wind speed.

$G_{\omega/V}(s)$ have the same characteristic equation, which means the same bandwidth and damping. However, the lead compensation links involved in the transfer functions are different and thereby lead to different frequency characteristics. In order to make the electrical power smoother, the bandwidth of $G_{P/V}(s)$ should be reduced as much as possible, while the precondition is that the wind turbine should always be kept in the stable region. Fig. 4(a)indicates the mechanical torque as a function of the rotating speed. The curve L_1 is composed of the

maximum torque points at each wind speed. The right side of L_1 is called the stable region, because $\frac{dT_m}{d\omega_m} < 0$ so the motion of the wind turbine will be damped (see Eqn. (8)). The left side of L_1 is called the unstable region, since $\frac{dT_m}{d\omega_m} > 0$ so the motion of the wind turbine will be enhanced (see Eqn. (8)). If the wind turbine is in the unstable region and $\frac{d\omega_m}{dt} > 0$, the wind turbine will speed up and get to the stable region. But if $\frac{d\omega_m}{dt} < 0$ when the wind turbine is in the unstable region, the wind turbine will speed down until it stops, which is not expected unless it is below the cut-in wind speed. With MPPT control, the static operation points of the wind turbine are all in the stable region. However, if the rotating speed has an overshoot as a response to the decrease of the wind speed, the wind turbine has the possibility to get to the unstable region with $\frac{d\omega_m}{dt} < 0$. As shown in Fig. 4(a), with a wind speed reduction ΔV_W, the wind turbine will go from A to B. The motion of the rotating speed is composed of $\Delta\omega_1$ and $\Delta\omega_{os}$, as illustrated in Fig. 4(b). The overshoot $\Delta\omega_{os}$ can be positive, but it should be lower than the gap between the MPPT curve and L_1 in order to avoid the undesired stop of the wind turbine. According to (13) and Fig. 4(b), it can be obtained,

$$|G_{\omega/V}(j\omega)| = \frac{\Delta\omega/\omega_{m0}}{\Delta V_W/V_{W0}} = \frac{(\Delta\omega_1 + \Delta\omega_{os})/\omega_{m0}}{\Delta V_W/V_{W0}} \quad (37)$$

Since $\Delta\omega_{os} \ll \Delta\omega_1$ is valid in the case a large wind speed reduction happens, the constraint for the stability of the wind turbine therefore can be obtained as, (in steady state of MPPT, the ratio between wind speed and rotating speed is fixed)

$$Max(|G_{\omega/V}(j\omega)|_{\omega=0\to\infty}) \leq \frac{\Delta\omega_1/\omega_{m0}}{\Delta V_W/V_{W0}} = 1 \quad (38)$$

According to (29), it is easy to obtain $|G_{\omega/V}(j\omega)|_{\omega=0} = 1$. Therefore, it can be concluded from (38) that no resonance is acceptable in $|G_{\omega/V}(j\omega)|$ for the stability of the wind turbine. Meanwhile, the resonance of $G_{P/V}(j\omega)$ and $G_{T/V}(j\omega)$ can also be studied by their maximum magnitudes, which are defined as,

$$M_P = \frac{Max(\left|G_{P/V}(j\omega)\right|_{\omega=0\to\infty})}{\left|G_{P/V}(j\omega)\right|_{\omega=0}} \quad (39)$$

$$M_\omega = \frac{Max(\left|G_{\omega/V}(j\omega)\right|_{\omega=0\to\infty})}{\left|G_{\omega/V}(j\omega)\right|_{\omega=0}} \quad (40)$$

$$M_T = \frac{Max(\left|G_{T/V}(j\omega)\right|_{\omega=0\to\infty})}{\left|G_{T/V}(j\omega)\right|_{\omega=0}} \quad (41)$$

where M_P, M_ω and M_T are relative magnitudes. Then the constraint for the stability of the wind turbine can be expressed as,

$$M_\omega \leq 1 \quad (42)$$

Substituting (27), (30) and (35), M_P, M_ω and M_T can be calculated as,

$$M_P = Max\left(\frac{\sqrt{\omega^2+\omega_{f1}^2}}{\sqrt{(\omega_0^2-\omega^2)^2+4\zeta^2\omega_0^2\omega^2}}\right)_{\omega=0\to\infty} \cdot \frac{\omega_0^2}{\omega_{f1}} \quad (43)$$

$$M_\omega = Max\left(\frac{\sqrt{\omega^2+\omega_{f2}^2}}{\sqrt{(\omega_0^2-\omega^2)^2+4\zeta^2\omega_0^2\omega^2}}\right)_{\omega=0\to\infty} \cdot \frac{\omega_0^2}{\omega_{f2}} \quad (44)$$

$$M_T = Max\left(\frac{\sqrt{\omega^2+\omega_{f3}^2}}{\sqrt{(\omega_0^2-\omega^2)^2+4\zeta^2\omega_0^2\omega^2}}\right)_{\omega=0\to\infty} \cdot \frac{\omega_0^2}{\omega_{f3}} \quad (45)$$

The maximum magnitudes as a function of $K_{i\omega}$ are illustrated in Fig. 5. When $K_{i\omega}$ is reduced, the bandwidth decreases, while the maximum magnitudes of $G_{P/V}(j\omega)$, $G_{T/V}(j\omega)$ and $G_{\omega/V}(j\omega)$ have different behaviours. Basically, those of $G_{P/V}(j\omega)$ and $G_{\omega/V}(j\omega)$ will increase, and that of $G_{T/V}(j\omega)$ will decrease. Therefore, it is concluded that, as the smoother electrical power is desired, the narrower bandwidth is required but at the same time more significant rotating speed variation will be introduced. Further, the electromagnetic torque or mechanical stress may not be increased or significantly increased with optimal design.

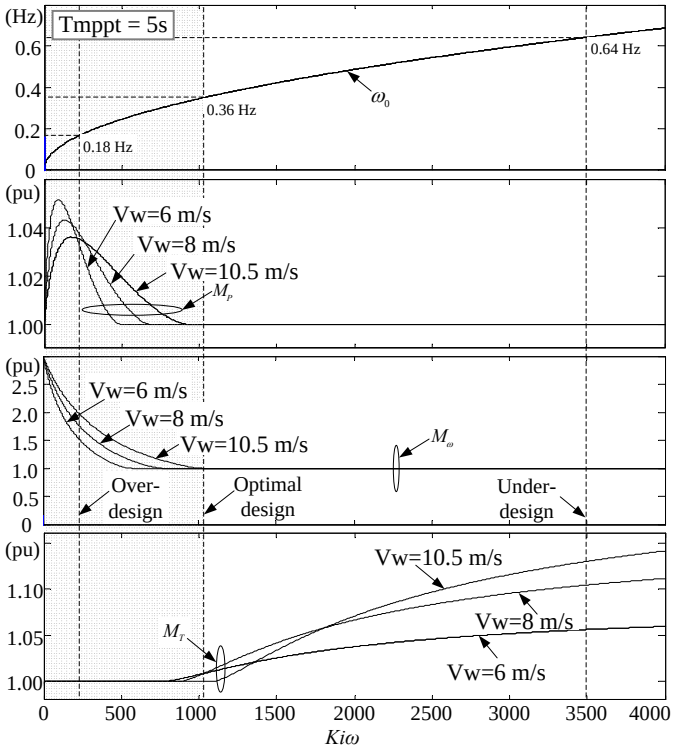

Fig. 5. The cut-off frequency and maximum magnitude of the transfer functions vs. K_{iw}.

TABLE I. A SET OF DESIGNS FOR THE ROTATING SPEED CONTROLLER.

	over-design	optimal design	under-design
$K_{p\omega}$	1150	5500	17500
$K_{i\omega}$	230	1100	3500

Based on Fig. 5, three designs are made for comparison, in terms of under-design, optimal design and over-design, which

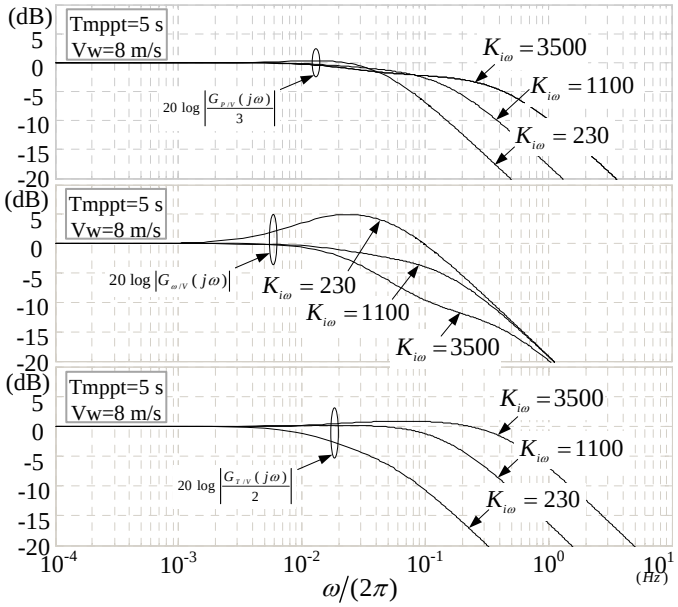

Fig. 6. Impact of $K_{i\omega}$ on magnitude of $G_{P/V}(s)$, $G_{T/V}(s)$ and $G_{\omega/V}(s)$.

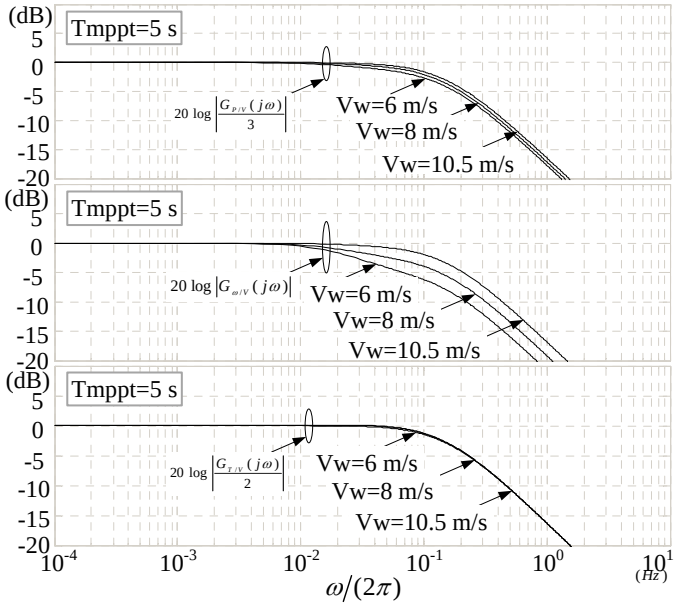

Fig. 7. Impact of V_W on magnitude of $G_{P/V}(s)$, $G_{T/V}(s)$ and $G_{\omega/V}(s)$.

are listed in Table I. In the optimal design, the minimum bandwidth is obtained and the constraint (Eqn. (42)) is still fulfilled. The plots in Fig. 5 are therefore divided into two parts by the optimal design, where the left and right sides are unstable and stable regions, respectively. Moreover, in optimal design the resonance exists in $G_{T/V}(j\omega)$, but the amplitude is only 1.02 pu. The corresponding frequency characteristics are then analysed by ***Bode Plots***, as shown in Fig. 6. In under-design and optimal design, there is no resonance in $G_{\omega/V}(s)$, but the bandwidth of $G_{P/V}(s)$ in the under-design is higher than optimal design. In the over-design, the bandwidth of $G_{P/V}(s)$ is narrower than optimal design, but the resonance of $G_{\omega/V}(s)$ is however large. Moreover, in the under-design a small resonance of $G_{T/V}(s)$ is observed. All of these match Fig. 5 very well. The sensitivity of the transfer functions with wind speeds is also studied, as indicated in Fig. 7. As seen, the wind speed has relatively more significant impact on $G_{\omega/V}(s)$, but it is still very small. Thus, the dimensionless transfer functions have good insistence in the whole operation region. The proposed design list of the rotating speed controller is further indicated in Table II.

It should be noted that the power fluctuations of the wind turbine mostly occur when the wind speed varies below the nominal wind speed, where both the current and the power are below their nominal values. When the wind speed is beyond the nominal value, the pitch control will be triggered to maintain a constant nominal power, and in this case the current of the wind power converter is limited to its nominal value. Therefore, with the proposed optimal design, the current will not go beyond the power converter rating.

TABLE II. THE DESIGN LIST OF THE ROTATING SPEED CONTROLLER.

Step 1	The dimensionless transfer functions $G_{P/V}(s)$, $G_{\omega/V}(s)$ and $G_{T/V}(s)$ are derived (see (26), (29) and (34)).
Step 2	Assuming $K_{p\omega} = T_{mppt} * K_{i\omega}$, the transfer functions $G_{P/V}(s)$, $G_{\omega/V}(s)$ and $G_{T/V}(s)$ become second-order, whose bandwidths are all proportional to $K_{i\omega}$.
Step 3	The stability condition is derived as following $Max\|G_{\omega/V}(j\omega)\| \leq \|G_{\omega/V}(j\omega)\|_{\omega=0}$ by which the minimum value of $K_{i\omega}$ is obtained. Afterwards, $K_{p\omega}$ is calculated as $K_{p\omega} = T_{mppt} * K_{i\omega}$.
Step 4	The response of the wind power to the wind speed variation is then checked at various wind speeds in frequency domain. Moreover, the response of the torque to the wind speed variation can also be evaluated by using $G_{T/V}(s)$.

IV. IMPACT OF THE OTHER PARAMETERS ON POWER LEVELLING

In order to get a better understanding of using the inertia energy for power levelling, the impact of the other parameters are also studied. From control point of view, the time constant of the MPPT control T_{mppt}, which is the longest one in the control system, could be one of the critical parameters. Another important parameter is the rotor inertia J since it dominates the capacity of the inertia energy. A case study is done, where T_{mppt} or J have different values for each case. The optimal design is obtained for each case following the method proposed above. The ***Bode Plots*** of the transfer functions with the optimal design are then used to analyze the impact of T_{mppt} and J.

A. Impact of the time constant T_{mppt}

The time constant T_{mppt} is set to be 5 s, 1 s and 0.1 s, respectively. The corresponding ***Bode Plots*** of the transfer functions with the optimal design are shown in Fig. 8. When

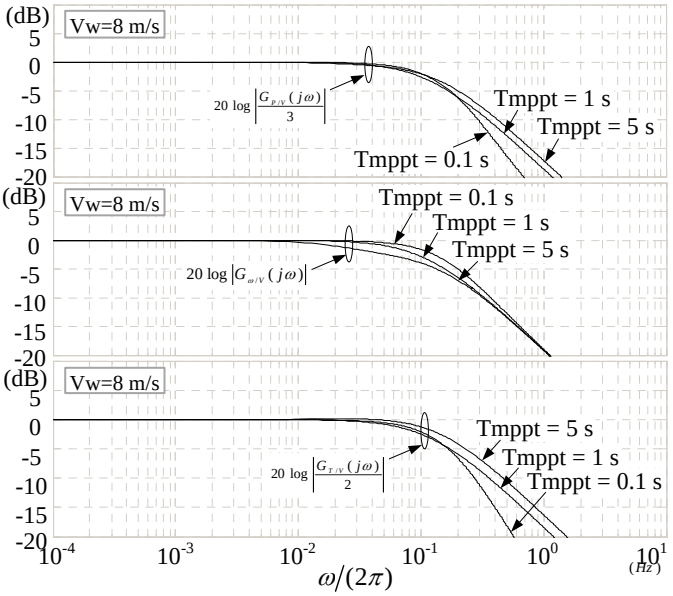

Fig. 8. Impact of time constant T_{mppt} on magnitude of $G_{P/V}(s)$, $G_{T/V}(s)$ and $G_{\omega/V}(s)$.

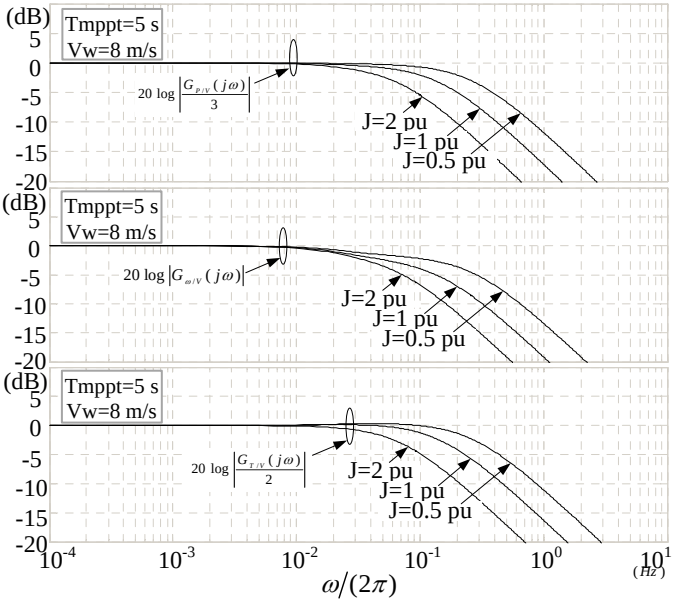

Fig. 9. Impact of inertia J on magnitude of $G_{P/V}(s)$, $G_{T/V}(s)$ and $G_{\omega/V}(s)$.

T_{mppt} is reduced, the bandwidth of $G_{P/V}(s)$, $G_{T/V}(s)$ and $G_{\omega/V(s)}$ will decrease. However, the reduction of T_{mppt} from 5 s to 0.1 s only influences the performance of power levelling slightly. Therefore, T_{mppt} is not a critical parameter from power levelling point of view.

B. Impact of the inertia moment J

The inertia of moment J is set to be 2 pu, 1 pu and 0.5 pu, respectively, where the value of 1 pu can be found in Appendix A. The corresponding ***Bode Plots*** of the transfer functions with the optimal design are shown in Fig. 9. When J is doubled, the bandwidth of $G_{P/V}(s)$, $G_{T/V}(s)$ and $G_{\omega/V(s)}$ will be half of the previous value. As a consequence, the inertia of moment J is very important for the power levelling and larger inertia can lead to smoother power .

V. Simulation Results

A wind power system model is built in Simulink/PLECS, where the modelling in Section II and the parameters in Appendix A are followed. As seen in Fig. 10 and Fig. 11, simulation of the wind turbine is first done with 5 s and 40 s wind turbulences, respectively, to verify the frequency characteristics of the proposed method. With the 5 s (0.2 Hz) wind turbulence, the over-design shows the best performance for power levelling as well as the torque levelling, where the optimal design followed. But with the 40 s (0.025 Hz) wind turbulence, the wind turbine with over-design gets to the unstable region gradually until it stops. This is because at 0.2 Hz the amplitude of $G_{\omega/V(s)}$ is below 1 pu, so the stability condition (42) is fulfilled, while at 0.025 Hz it is around 2 pu, which is beyond the constraint for stability and makes the system unstable (see Fig. 6).

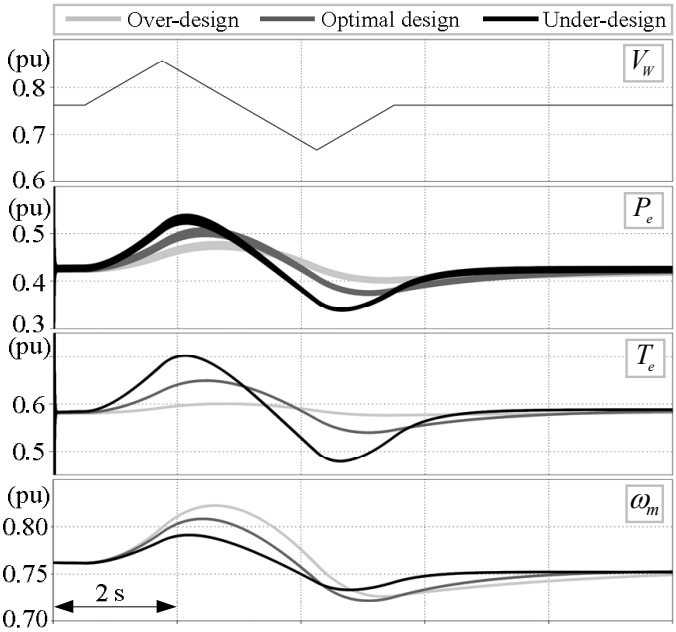

Fig. 10. Behaviour of the wind turbine with various design in a 5 s wind turbulence.

A roughness class 4 wind profile [32] is then employed to study the behaviour of the wind turbine, as shown in Fig. 12. The optimal design leads to smoother power and torque than under-design, and its rotating speed has more significant variation. The power coefficient C_P is also influenced by the various designs, where the under-design has the highest C_P and the optimal design just followed. Nevertheless, C_P is above 0.95 pu with the optimal design. The over-design again has the smoothest power and torque. Despite, the lowest C_P and stability issue of over-design make it unacceptable.

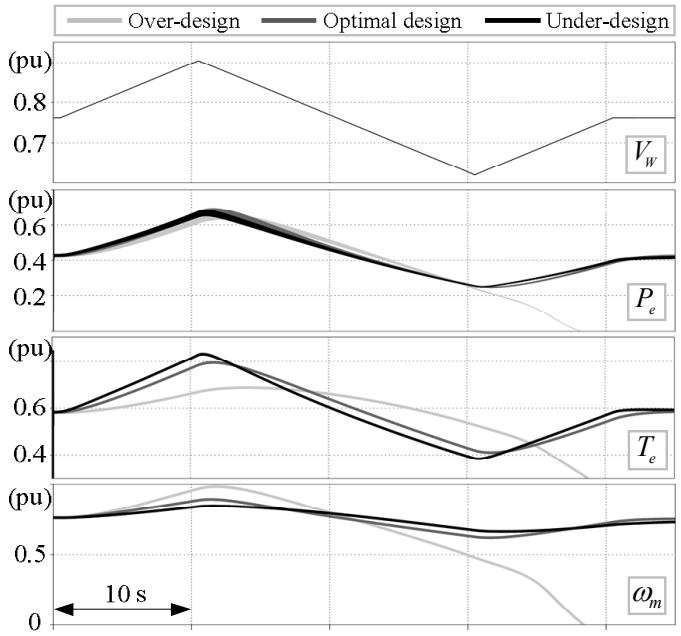

Fig. 11. Behaviour of the wind turbine with various design in a 40 s wind turbulence.

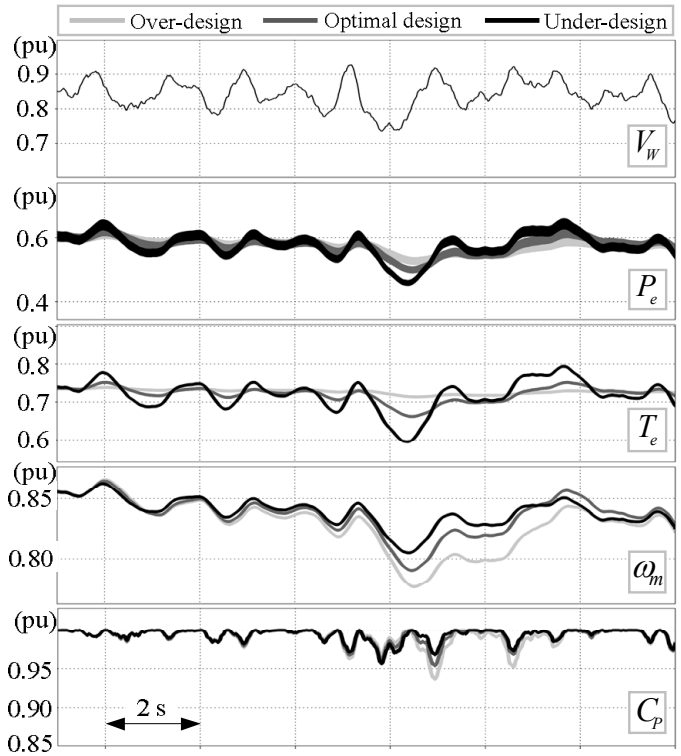

Fig. 12. Behaviour of the wind turbine with various design in a roughness class 4 wind profile.

VI. Conclusion

The transfer functions from the wind speed to electrical power, electromagnetic torque and rotating speed are built, based on which the rotating speed controller is designed for power levelling in the frequency domain. Moreover, the impact of other parameters on the power levelling, including the time constant of MPPT and the rotor inertia, is also studied. With the proposed optimal design, the power is smoothed significantly as well as the torque, and the performance of MPPT is weakened slightly. On the other hand, the rotating speed varies more intensely, but the wind turbine is still in the stable region since the constraint of rotating speed for stability is followed. It is also found that the rotor inertia instead of the time constant of MPPT is a critical parameter for the power levelling.

Appendix A

TABLE III. Parameters of the Wind Power System.

Parameter	Symbol	Value
Nominal power	$\boldsymbol{P_n}$	3 MW
Nominal wind speed	$\boldsymbol{V_{Wn}}$	10.5 m/s
Nominal rotating speed	$\boldsymbol{\omega_{mn}}$	15.3 rpm
Nominal torque	$\boldsymbol{T_{mn}}$	1.86 $MN \cdot m$
Inertia of moment	$\boldsymbol{J}$	3.81 $Mkg \cdot m^2$
Radius of the blade	$\boldsymbol{R}$	53 m
Coefficients	$\boldsymbol{c_1 \sim c_6}$	0.5176, 116, 0.4 5 ,21, 0.0068
Air density	$\boldsymbol{\rho}$	1.225 kg/m^3
Flux induced by magnet	$\boldsymbol{\varphi}$	2.5 Wb
Inductance of the stator	$\boldsymbol{L_s}$	0.835 mH
Resistance of the stator	$\boldsymbol{R_s}$	6 $m\Omega$
Number of pole pairs	$\boldsymbol{p}$	120
Time constant of MPPT	$\boldsymbol{T_{mppt}}$	5 s
Current controller	$\boldsymbol{G_{si}}$	$0.9 + \frac{809}{s}$

References

[1] F. Blaabjerg, Z. Chen, and S. B. Kjaer, "Power electronics as efficient interface in dispersed power generation systems," *IEEE Trans. Power Electron.*, vol. 19, no. 5, pp. 1184–1194, 2004.

[2] Z. Chen, J. M. Guerrero, and F. Blaabjerg, "A review of the state of the art of power electronics for wind turbines," *IEEE Trans. Power Electron.*, vol. 24, no. 8, pp. 1859–1875, 2009.

[3] M. Liserre, R. Cardenas, M. Molinas, and J. Rodriguez, "Overview of multi-mw wind turbines and wind parks," *IEEE Trans. Ind. Electron.*, vol. 58, no. 4, pp. 1081–1095, 2011.

[4] Wind power produced more than half the electricity in spain during the early morning hours, spain, nov 2009. http://www.ree.es/. [Online; accessed 12-August-2014].

[5] Danish wind industry association, europe. http://www.windpower.org/en/policy/europe.html/. [Online; accessed 12-August-2014].

[6] Y. Song and B. Wang, "Survey on reliability of power electronic systems," *IEEE Trans. Power Electron.*, vol. 28, no. 1, pp. 591–604, 2013.

[7] I. Swan, A. Bryant, P. A. Mawby, T. Ueta, T. Nishijima, and K. Hamada, "A fast loss and temperature simulation method for power converters, part ii: 3-d thermal model of power module," *IEEE Trans. Power Electron.*, vol. 27, no. 1, pp. 258–268, 2012.

[8] Y. Firouz, M. T. Bina, and B. Eskandari, "Efficiency of three-level neutral-point clamped converters: analysis and experimental validation of power losses, thermal modelling and lifetime prediction," *IET Power Electron.*, vol. 7, no. 1, pp. 209–219, 2014.

[9] Abb application note. Load-cycling capability of HiPak IGBT, 2012.

[10] C. Busca, R. Teodorescu, F. Blaabjerg, S. Munk-Nielsen, L. Helle, T. Abeyasekera, and P. Rodriguez, "An overview of the reliability prediction related aspects of high power igbts in wind power applications," *Microelectronics reliability*, vol. 51, no. 9-11, pp. 1903–1907, 2011.

[11] A. Abedini and A. Nasiri, "Applications of super capacitors for pmsg wind turbine power smoothing," *in Proc. of IEEE-IECON' 2008*, pp. 3347–3351, 2008.

[12] T. Kinjo, T. Senjyu, N. Urasaki, and H. Fujita, "Output levelling of renewable energy by electric double-layer capacitor applied for energy storage system," *IEEE Trans. Energy Convers.*, vol. 21, no. 1, pp. 221–227, 2006.

[13] C. Abbey and G. Joos, "Supercapacitor energy storage for wind energy applications," *IEEE Trans. Ind. Appl.*, vol. 43, no. 3, pp. 769–776, 2007.

[14] F. Diaz-Gonzalez, F. D. Bianchi, A. Sumper, and O. Gomis-Bellmunt, "Control of a flywheel energy storage system for power smoothing in wind power plants," *IEEE Trans. Energy Convers.*, vol. 29, no. 1, pp. 204–214, 2014.

[15] W. Li, G. Joos, and C. Abbey, "A parallel bidirectional dc/dc converter topology for energy storage systems in wind applications," *in Proc. of IEEE-IAS' Annual Meeting 2007*, pp. 179–185, 2007.

[16] T. Brekken, A. Yokochi, A. von Jouanne, Z. Yen, H. Hapke, and D. Halamay, "Optimal energy storage sizing and control for wind power applications," *IEEE Trans. Sustainable Energy*, vol. 2, no. 1, pp. 69–77, 2011.

[17] Z. Qin, M. Liserre, F. Blaabjerg, and H. Wang, "Energy storage system by means of improved thermal performance of a 3 mw grid side wind power converter," *in Proc. of IECON' 2013*, pp. 736–742, 2013.

[18] N. W. Miller. Ge experience with turbine integrated battery energy storage. http://www.ieee-pes.org/presentations/gm2014/PESGM2014P-000717.pdf. [Online; accessed 23-Jan-2014].

[19] The cost of wind energy: Tradeoffs between energy storage and transmission. http://chicagopolicyreview.org/2014/05/27/the-cost-of-wind-energy-tradeoffs-between-energy-storage-and-transmission/. [Online; accessed 23-Jan-2015].

[20] T. Senjyu, R. Sakamoto, N. Urasaki, T. Funabashi, Hideki, and H. Sekine, "Output power leveling of wind turbine generator for all operating regions by pitch angle control," *IEEE Trans. Energy Convers.*, vol. 21, no. 2, pp. 467–475, 2006.

[21] A. Uehara, A. Pratap, T. Goya, T. Senjyu, A. Yona, N. Urasaki, and T. Funabashi, "A coordinated control method to smooth wind power fluctuations of a pmsg-based wecs," *IEEE Trans. Energy Convers.*, vol. 26, no. 2, pp. 550–558, 2011.

[22] X. Yuan, F. Wang, D. Boroyevich, Y. Li, and R. Burgos, "Dc-link voltage control of a full power converter for wind generator operating in weak-grid systems," *IEEE Trans. Power Electron.*, vol. 24, no. 9, pp. 2178–2192, 2009.

[23] T. Senjyu, Y. Ochi, Y. Kikunaga, M. Tokudome, and E. B. Muhando, "Output power leveling of wind generation system using inertia of wind turbine," *in Proc. of IEEE-ICSET*, pp. 1217–1222, 2008.

[24] A. M. Howlader, N. Urasaki, T. Senjyu, A. Yona, T. Funabashi, and A. Y. Saber, "Output power leveling of wind generation system using inertia for pm synchronous generator," *in Proc. of IEEE-PEDS*, pp. 1289–1294, 2009.

[25] A. Uehara, B. Asato, T. Goya, T. Senjyu, A. Yona, T. Funabashi, and C.-H. Kim, "Output power smoothing of pmsg-based wind energy conversion system," *in Proc. of IEEE-IPEC*, pp. 128–133, 2010.

[26] N. P. G. van Deelen, A. Jokic, P. P. J. van den Bosch, and R. M. Hermans, "Exploiting inertia of wind turbines in power network frequency control: a model predictive control approach," *in Proc. of IEEE-CCA*, pp. 1309–1314, 2011.

[27] T. Luu, A. Abedini, and A. Nasiri, "Power smoothing of doubly fed induction generator wind turbines," *in Proc. of IEEE-IECON' 2008*, pp. 2365–2370, 2008.

[28] L. Ran, J. R. Bumby, and P. J. Tavner, "Use of turbine inertia for power smoothing of wind turbines with a dfig," *in Proc. of ICHQP' 2004*, pp. 106–111, 2004.

[29] A. Abedini, G. Mandic, and A. Nasiri, "Wind power smoothing using rotor inertia aimed at reducing grid susceptibility," *in Proc. of IEEE-IECON' 2008*, pp. 1445–1451, 2008.

[30] C. Luo, H. Banakar, B. Shen, and B.-T. Ooi, "Strategies to smooth wind power fluctuations of wind turbine generator," *IEEE Trans. Energy Convers.*, vol. 22, no. 2, pp. 341–349, 2007.

[31] D. Holmes, T. Lipo, B. McGrath, and W. Kong, "Optimized design of stationary frame three phase ac current regulators," *IEEE Trans. Power Electron.*, vol. 24, no. 11, pp. 2417–2426, 2009.

[32] Danish wind industry association, wind turbine power calculator. http://www.motiva.fi/myllarin_tuulivoima/windpower%20web/en/tour/wres/pow/index.htm/. [Online; accessed 22-July-2014].

Zian Qin (S'13) received his B.Eng and M.Eng from the Beihang University and Beijing Institute of Technology, Beijing, China, in 2009 and 2012, respectively. He is now working towards his Ph.D in Aalborg University, Aalborg, Denmark. In 2014, he was a Visiting Scientist with the Institute for Power Generation and Storage Systems (PGS), Aachen University, Aachen, Germany, where he focused on the wind power generation.

Frede Blaabjerg (S'86−M'88−SM'97−F'03) was with ABB-Scandia, Randers, Denmark, from 1987 to 1988. From 1988 to 1992, he was a Ph.D. Student with Aalborg University, Aalborg, Denmark. He became an Assistant Professor in 1992, an Associate Professor in 1996, and a Full Professor of power electronics and drives in 1998. His current research interests include power electronics and its applications such as in wind turbines, PV systems, reliability, harmonics and adjustable speed drives. He has received 15 IEEE Prize Paper Awards, the IEEE PELS Distinguished Service Award in 2009, the EPE-PEMC Council Award in 2010, the IEEE William E. Newell Power Electronics Award 2014 and the Villum Kann Rasmussen Research Award 2014. He was an Editor-in-Chief of the IEEE TRANSACTIONS ON POWER ELECTRONICS from 2006 to 2012. He has been Distinguished Lecturer for the IEEE Power Electronics Society from 2005 to 2007 and for the IEEE Industry Applications Society from 2010 to 2011.

Poh Chiang Loh received his B.Eng (Hons) and M.Eng from the National University of Singapore in 1998 and 2000 respectively, and his Ph.D from Monash University, Australia, in 2002, all in electrical engineering. His interests are in power converters and their grid applications.